SIMULATION OF CLOUD RADIATIVE FORCING WITH THE ECMWF MODEL

Michèle Vesperini[1], Jean-Jacques Morcrette[2], Yves Fouquart[1]

[1]Laboratoire d'Optique Atmosphérique, 59655 - Villeneuve d'Ascq, France
[2]E.C.M.W.F., Shinfield Park, Reading, Berkshire, RG2 9AX, U.K.

Introduction

Clouds are the main modulators of the Earth's surface and tri-dimensional atmospheric radiative heating. Due to the diversity of atmospheric conditions that produce clouds, a multitude of cloud types can be distinguished depending on their height, depth, size, water or ice content. Moreover, clouds are often related to processes which are subgrid scale for the present general circulation models (GCMs). In GCMs, the cloud parameterization aims at describing most of the actual cloud types in terms of a small number of more likely cloud systems (e.g., convective clouds, low-, medium-, and high-level layered clouds). From a set of predictors directly derived from the large-scale flow and thermodynamic state, the cloud parameterization diagnoses (or prognoses) a cloud with its associated cover, height, depth and water content. Corresponding optical properties are derived that are inputs to the radiation scheme.

In his recent review, Mitchell (1989) pointed out that a good representation of the future climatic conditions requires a model with a realistic cloud scheme, not only with regards to horizontal fractional cover but also to other geometrical and radiative parameters. Furthermore, the present model representation of clouds, cloud water, and cloud radiative properties as functions of large-scale variables is extremely crude. As such, clouds are certainly one of the major sources of uncertainties in the determination of climate sensitivity (Cess et al., 1989).

As both the real cloud generation processes and optical properties are only

roughly known, it is worthwhile to check the present model cloud parameterizations for what is readily available: the impact of clouds on the radiation fields at the top of the atmosphere (TOA). These quantities have been observed from satellites for about three decades and are basic outputs of most GCMs.

Since November 1984, the Earth Radiation Budget Experiment (ERBE; Barkstrom, 1984; Barkstrom and Smith, 1986) has been providing well-calibrated broadband radiance measurements (in the 0.2 to 5 μm shortwave and 5 to 200 μm longwave range). The presence of a scene identification index in the ERBE data (Smith et al., 1986) allows to distinguish the different underlying surfaces (ocean, land, desert, snow) and cloudy states of the atmosphere above (clear, partially or mostly cloudy, overcast). Using such a discrimination, "state-of-the-art" bi-directional reflectances (Smith et al., 1986) are then used to convert the radiances into TOA irradiances. This index is also central in the concept of cloud radiative forcing (i.e., the difference between clear-sky and cloudy radiative fluxes) first introduced by Coakley and Baldwin (1984).

Most GCM validations have been performed on model climates simulated on a multi-year temporal scale (Smith, 1989; Kielh and Ramanathan, 1990). On the contrary, this paper is based on a 30-day forecast and thus the model results are not as divorced from the initial conditions.

In the following, the radiative fluxes (shortwave SW, and longwave LW, and corresponding cloud forcings) derived from ERBE measurements are compared to similar quantities produced by the European Centre for Medium-range Weather Forecasts (ECMWF) operational model. Morcrette (1990a) showed that the physics package implemented in May 1989 in the ECMWF operational model gives a more realistic representation of the radiative components and corrected some of the model systematic errors. This allows us to compare observed and simulated monthly averaged fields. The new radiation scheme is based on an updated version of the radiation codes originally developed at the University of Lille (Fouquart and Bonnel, 1980; Morcrette and Fouquart, 1986; Morcrette et al., 1986). Extensive comparisons of this radiation package with detailed radiation models have recently been carried out for various clear sky and cloudy standard atmospheres in the framework of the Intercomparison of Radiation Codes in Climate Models (ICRCCM) program (Luther et al., 1988). They show

maximum local errors in longwave and shortwave clear sky heating rates of 0.15 and 0.10 K day^{-1}, respectively, corresponding to a better than 5 percent agreement on both longwave and shortwave clear sky atmospheric absorptions. Agreement of about 1 % is obtained on clear-sky longwave and shortwave fluxes at the top of the atmosphere. Full results can be found in Morcrette (1990b).

1. Methodology

1.1. Model experiment

The experiment is a 30-day forecast, run from analyzed initial conditions for 1 January 1986 using a T63 version of the ECMWF operational model (cycle 34 of the libraries). This triangular truncation gives a $(1.875^{\circ})^2$ grid for the physical processes. The sea surface temperature is the analyzed field produced by NMC for 1 January 1986 and it is kept fixed over the length of integration. The cloud scheme produces convective, high-, medium-, and low-level clouds following Slingo (1987). The model includes the mass-flux convection scheme of Tiedtke (1989) and the radiation scheme of Morcrette (1990). The radiation scheme accounts for the diurnal cycle of insolation. The full radiation scheme is called every 3 hours, but radiation fields are updated at every time-step (Δt = 1350 s) accounting for any variation in solar zenith angle (in the SW scheme) and black-body temperature (in the LW scheme). Extra radiation diagnostics have been added to the operational diagnostics package, to keep track of the clear-sky SW and LW fluxes that would be obtained assuming radiatively transparent clouds over the whole globe. These extra fields are stored every 9 hours to sample an average diurnal cycle over the month.

1.2. Satellite data

The satellite data are the so-called ERBE S9 products including the daily and monthly means of the clear-sky and total fluxes, averaged over 2.5° latitude x 2.5° longitude grid. The averaging of the data over the day must account not only for the meteorological variability but also for the systematic variation of albedo with solar zenith angle, and the concomitant changes in emitted longwave radiation associated with the surface heating and cooling. A good sampling of these processes should require, for each $(2.5^{\circ})^2$ region, a full matrix with hours of the day as columns and days of the month as rows. Then,

the daily means could be computed by adding up the regional fluxes of all hour boxes in a row and dividing by 24. However, even a three-satellite system like ERBE cannot give more than 6 measurements per 24-hour period. Moreover, the ERBE system has never been working with more than two satellites. For example, the sun-synchronous NOAA-9 and ERBS with its precessing orbit have given two fixed hour and two variable time measurements per day (cf. Figure 1). In order to compensate for this poor sampling, the radiative fields have been interpolated in each hour box. For LW fluxes, a simple linear interpolation is used, except over land and deserts where the high range of diurnal temperature variations is modelled with a trigonometric interpolation; for SW fluxes, the interpolation accounts for the diurnal variation of the albedo of the underlying surfaces according to the scene type. No reliable estimate of the bias due to this interpolation procedure is available yet.

The daily values of the clear-sky fluxes are computed using similar procedures applied on only those measurements sorted out as clear sky. At night, the identification of clouds based on a maximum likelihood estimator technique applied on a pair of SW/LW radiance measurements cannot be applied. Thus, due to a limited knowledge of the surface temperature variations, the number of retrieved clear sky observations is really poor. As over the land and desert scenes, the diurnal longwave range is relatively high, this smaller number of clear sky samples during nighttime is likely to give a bias in the interpolated result. In case of poor clear sky sampling, the clear sky daily mean is not made available. That is why the daily LW and SW clear-sky values over most of the continents is absent from the ERBE S9 data, as shown in the observed LW and SW cloud forcing field of Figures 3a and 4a. The scene identification allows a residual cloudiness of 5 %. The effect of this potential contamination is maximum for SW clear sky fluxes over the oceans because the reflectance contrast between cloud and surface is greater than over brighter land surfaces. Ramanathan et al. (1989) have investigated this issue using more stringent scene identification procedures over ocean based on spatial homogeneity criteria. This yielded lower clear clear sky albedos and larger LW fluxes. However the bias on clear sky albedo and OLR is only 0.8 % and 4 W m^{-2}, respectively, on an instantaneous basis.

ERBE day-hour matrix for January 1986 (equator, Greenwich meridian) shaded values correspond to NOOA-9 or ERBS observations.

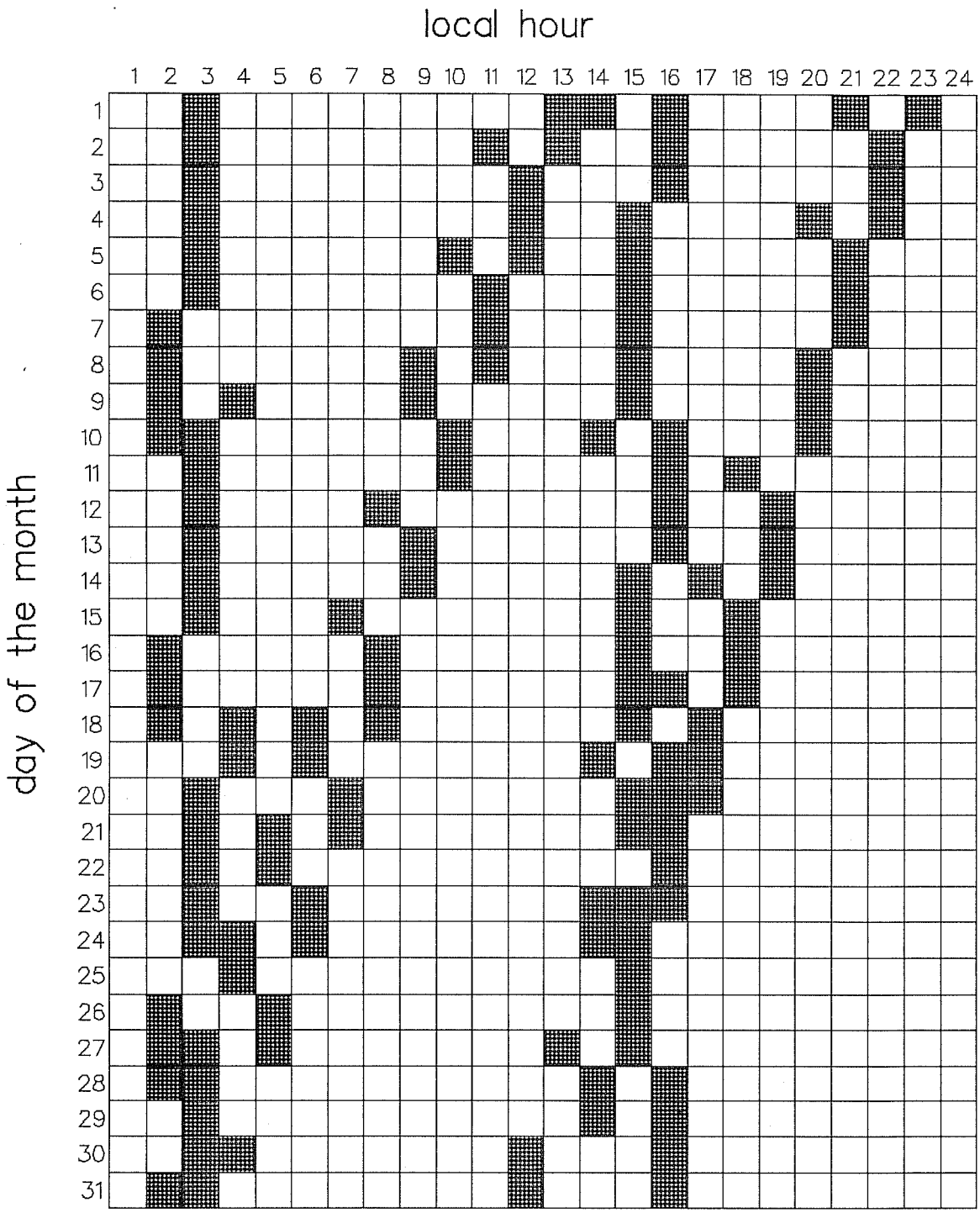

Figure 1: The day-hour matrix of occurrence of ERBE observations for January 1986.

1.3. The cloud radiative forcing

The clcud radiative forcing (CF), first introduced by Coakley and Baldwin (1984), is computed as the difference between the flux which would be measured without clouds (clear refer to clear-sky conditions) and the total flux (total refer to mixed clear-sky and cloudy conditions averaged over the scene):

$$CF = F_{clear} - F_{total} + Q_{total} - Q_{clear}$$

where F is the outgoing longwave flux and Q is the net shortwave flux at the top of the atmosphere. It can be rewritten as

$$CF = A_c \, (F_{clear} - F_{cloud} + Q_{cloud} - Q_{clear})$$

with A_c the cloudiness and cloud refer to overcast conditions. F_{clear} varies primarily with the surface temperature and emissivity and the vertically integrated water vapor amount, Q_{clear} varies with the solar irradiance and the surface albedo. The longwave overcast flux decreases when cloud height and emissivity increases whereas the shortwave overcast flux depends on solar zenith angle and cloud optical thickness. The first-order modulator of the cloud forcing is clearly the cloud cover. The other parameters have a more subtle impact. In the model, the cloud optical properties are linked to the diagnosed liquid water path (LWP) through the longwave emissivity ε and the shortwave optical thickness δ

$$\varepsilon = 1 - e^{-kLWP}$$

$$\delta = \frac{3 \, LWP}{2 \, r_e}$$

where k is the mean over the whole longwave spectrum of the mass absorption coefficient of liquid water, and r_e is the effective radius of the cloud droplets. With such a parameterization of the cloud optical properties, the longwave and shortwave cloudy fluxes are consistent as ε and δ are both linked to the same LWP.

Then, by comparing the observed longwave (warming term) and shortwave (cooling term) forcings with the equivalent model diagnostics, we can get some insight

on deficiencies in the model representation of the cloud and radiation interactions.

2. Results

2.1. Outgoing longwave radiation and cloud longwave forcing

The comparison between the monthly means of model and observed outgoing longwave flux (Figure 2) shows larger maxima in the model fields than in the observations (310 instead of 290 W m^{-2}). One explanation is that the model simulated clear sky atmosphere is too transparent as also noticed in a comparison of observed and simulated radiances (Morcrette and Fouquart, 1989). First, absorption by trace gases (N_2O, CH_4 and CFC) and aerosols is not included in the radiation code; comparisons with a narrow-band model results (Morcrette and Fouquart, 1985) show that this absorption can account for up to 8 W m^{-2}; second, the atmosphere may be too dry. Comparisons with analyses show the planetary boundary layer to be too dry. Over the subtropical oceans, it can be linked to a lack of evaporation in case of low winds (< 5 m s^{-1}) (Beljaars and Miller, 1990). As the surface longwave emissivity is set to 0.995 without any geographical variations, it can result in an overestimation of the model longwave flux, specially over the desert areas. The comparisons also shows model minima that are too low in the tropics (190 instead of 210 W m^{-2}), for example over Brazil, East Africa and Madagascar. This feature is generally associated with areas of strong convective activity producing a large cover of optically thick high clouds.

The effect of these high clouds shows up even more in the longwave cloud forcing (Figure 3). In the observations, the black areas correspond to areas with not enough clear sky measurements during the month to retrieve reliable monthly clear sky fluxes (cf. section 1.2). Too many, too high or too optically thick clouds are seen in the South Pacific Convergence Zone (SPCZ) and offshore Guyana where the model maintains a spurious convective activity (not present in the observations). In those areas, the longwave cloud forcing is too large by up to 20 W m^{-2}. In the winter monsoon region, the model clouds are less well organized than the observed ones. This corresponds to systematic error of the ECMWF model recently linked to the deficient evaporation over the tropical oceans in case of low winds (Beljaars and Miller, 1990). However, in

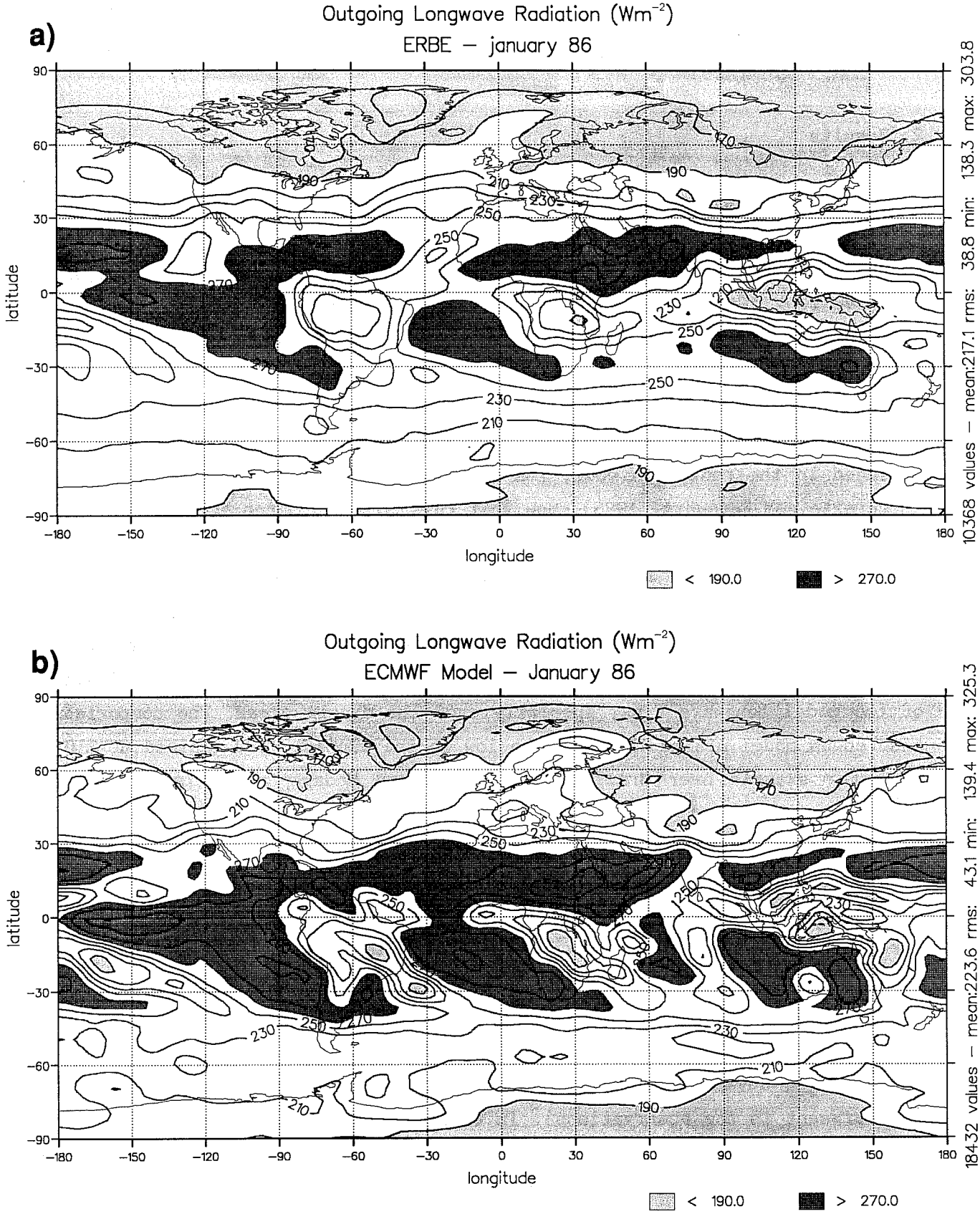

Figure 2: The monthly mean outgoing longwave radiation for January 1986: ERBE observations on top (fig.2a), ECMWF model field below (Fig. 2b). Interval is 20 W m^{-2}. Values below 190 W m^{-2} and above 270 W m^{-2} are shaded.

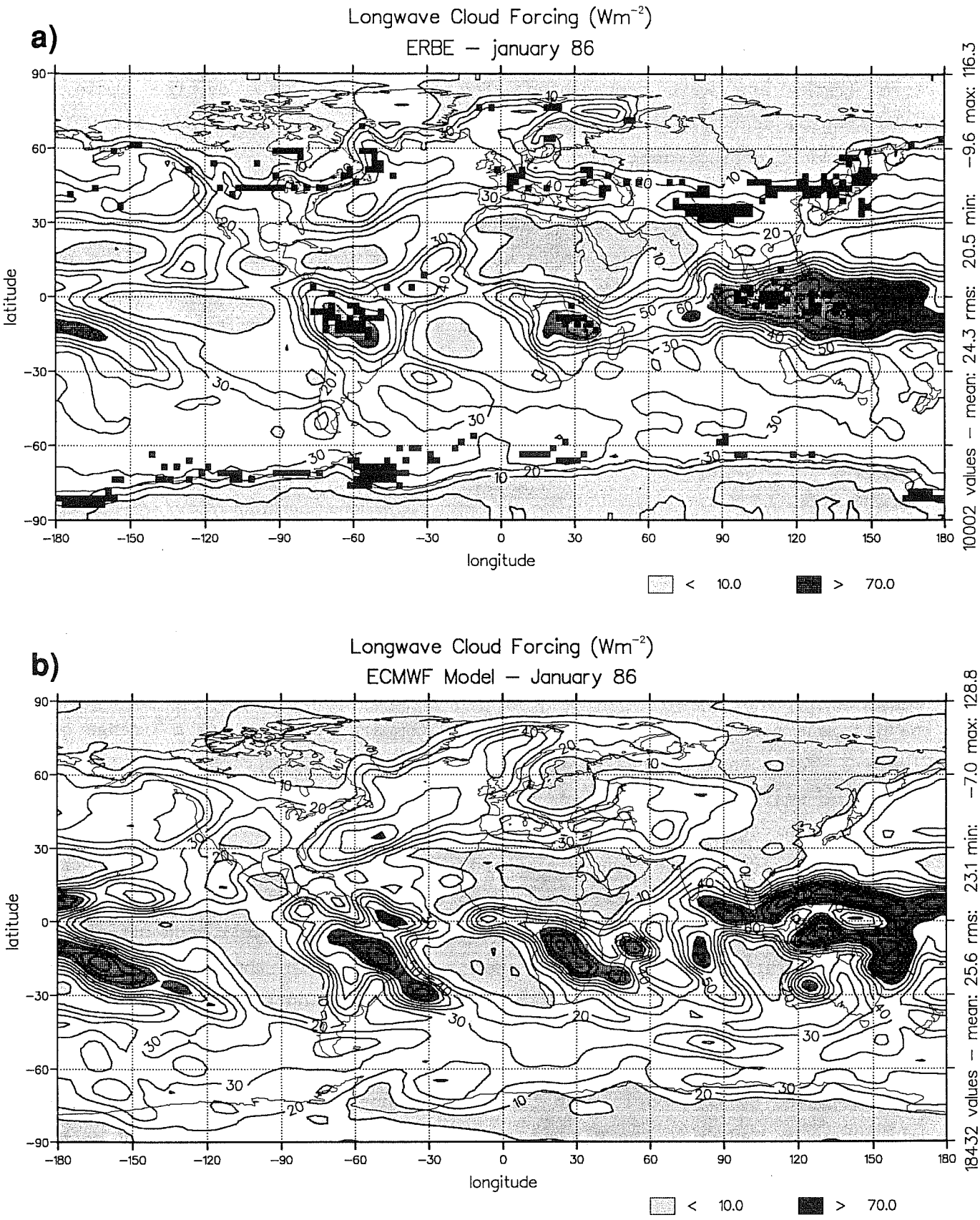

Figure 3: The monthly mean longwave cloud forcing for January 1986: ERBE observations on top (fig.3a), ECMWF model field below (Fig. 3b). Interval is 10 W m^{-2}. Values below 10 W m^{-2} and above 70 W m^{-2} are shaded. Black squares in Fig. 3a indicate missing clear-sky observations.

this region, the model longwave cloud forcing is in better agreement with the observations (to about 10 W m^{-2}). The North-West Pacific and North-Atlantic storm tracks are well represented. The maximum of LWCF on the eastern North-America seaboard and the sea-land contrast around Scandinavia are well located and of correct amplitude.

Figures 2 and 3 also show the signature of the missing low level stratiform clouds on the western façades of Peru, Angola and Australia. Observations of longwave cloud forcing are in the 20 W m^{-2} range whereas the model values correspond to clear sky atmospheres (< 10 W m^{-2}). These clouds result from a delicate balance between large-scale subsidence and typically sub-grid processes such as cloud top radiative cooling, entrainment of warmer and drier air from above, and turbulent buoyancy fluxes. At present no GCM-type cloud scheme is able to account correctly for these interactions.

2.2. Shortwave field

Previous results are confirmed when comparing observed and model shortwave cloud forcing (Figure 4). They also put some extra light on other deficiencies of the model. In this figure, the lack of stratiform cloudiness west of the southern hemisphere continents shows more strongly than in the longwave range. The discrepancies are in the 30 W m^{-2} range compared to the 10 W m^{-2} range of Figure 3. This confirms that it is not only a problem of improper cloud height but of too small or inexistent low cloud cover.

As already seen in the longwave field, the convective activity over the tropical continents is generally well located, but the radiative effect of the convective clouds appear too high by 30 to 60 W m^{-2} over Brazil, and off-shore Guyana. Similarly, the radiative impact of clouds in the model is much stronger than observed in the monsoon area (Indonesia and the SPCZ).

The radiative effect of the 50°S-60°S latitude cloud belt is quite underestimated by the model, with local differences as high as 60 W m^{-2}. This deficiency is linked to the diagnostic formulation of the cloud liquid water content as a given fraction of the saturated mixing ratio of water vapor. Despite the improvement brought in May 1989 by the change of radiation scheme and cloud optical properties (Morcrette, 1990), the decrease of cloud liquid water content with increasing latitude (through cooler temperature of the

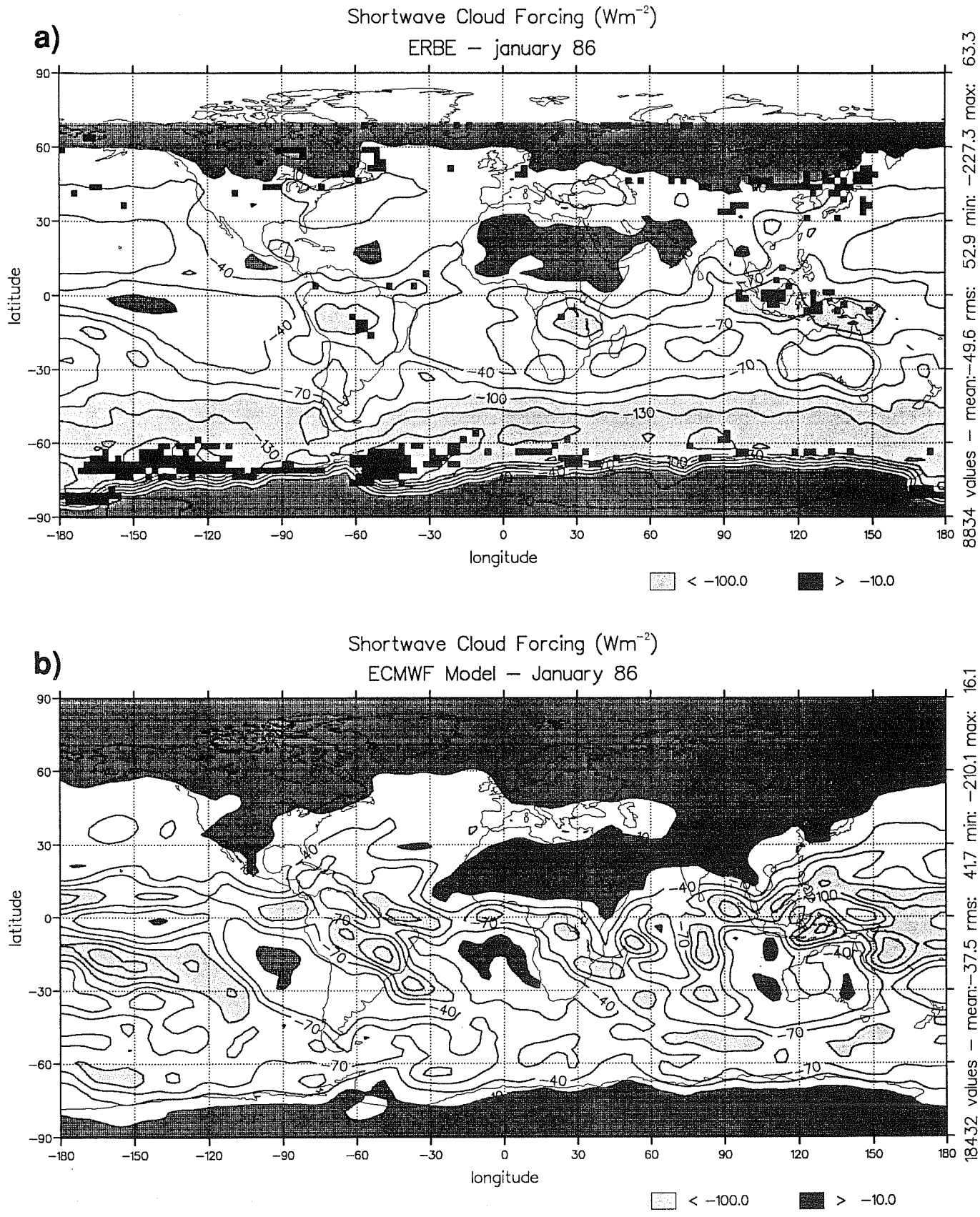

Figure 4: The monthly mean shortwave cloud forcing for January 1986: ERBE observations on top (fig.4a), ECMWF model field below (Fig. 4b). Interval is 30 W m^{-2}. Values below -100 W m^{-2} and above -10 W m^{-2} are shaded. Black squares in Fig. 4a indicate missing clear-sky observations.

environment) is still unrealistic. Here a prognostic formulation of the cloud liquid water content would certainly bring remedy to this problem.

The shortwave cloud forcing obviously depends on the clear-sky planetary albedo. Therefore, any deficiency in the modelling of the surface albedo will contribute to discrepancy between model and observations. Particularly, too low a surface albedo will enhance the model shortwave cloud forcing through an underestimated clear-sky upward flux. Model clear-sky upward shortwave fluxes (USW, shown in Figure 5) are slightly underestimated over the oceans and are strongly underestimated over most of the land and desert surfaces (by up to 30 W m^{-2} over Brazil, Africa and Australia). However, the discussion on regional aspects (section 3) shows that the large differences of Figure 4 cannot be fully attributed to this single problem.

2.3. Temporal variability

The extra radiation diagnostics fields have been stored every 9 hours of model integration. Therefore, a complete sampling of the daily cycle (assuming that 8 points separated by 3 hours are enough to correctly describe the diurnal variations of cloudiness and radiation fields) requires averaging data over 3 model days. From these 3-day averages, a standard deviation with respect to the monthly means of these 3-day samples can be computed. Obviously, the ERBE measurements have been processed consistently to obtain observed quantities to be compared to the model outputs. Then, a comparison of the observed and model fields obtained in this manner allows to study the temporal variability for time scales longer than 3 days.

Figure 6 shows the standard deviation of the OLR, σ(OLR), whereas Figure 7 shows the standard deviation of the upward shortwave radiation at TOA , σ(USW). In the observations, the larger values of standard deviation are found in the areas displaying the maximum in the cloud forcing, showing that variations in cloudiness are the main contributors to the variability of the radiation fields. Whilst some maxima of the model σ(OLR) occur roughly over the same regions as in the observations (Indian ocean, SPCZ, Brazil), the model field is much less organized and more spotty: this lack of spatial organization is evident in the *spatial* standard deviations of the monthly mean radiation components over characteristic areas shown in Table 1. Moreover, the model does not show any large values of σ(OLR) and σ(USW) in the monsoon area.

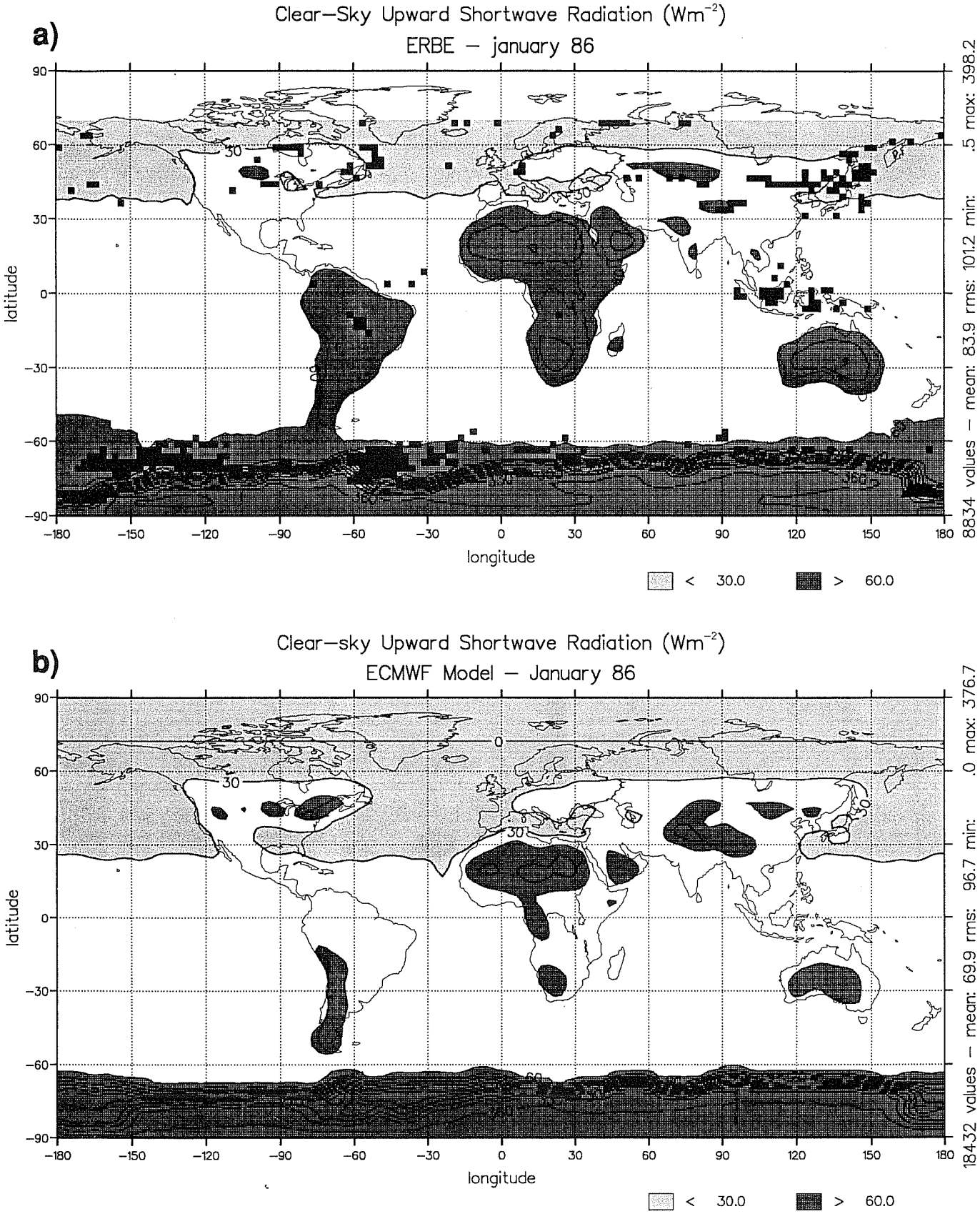

Figure 5: The monthly mean clear-sky upward shortwave radiation for January 1986: ERBE observations on top (fig.5a), ECMWF model field below (Fig. 5b). Interval is 30 W m^{-2}. Values below 30 W m^{-2} and above 60 W m^{-2} are shaded.

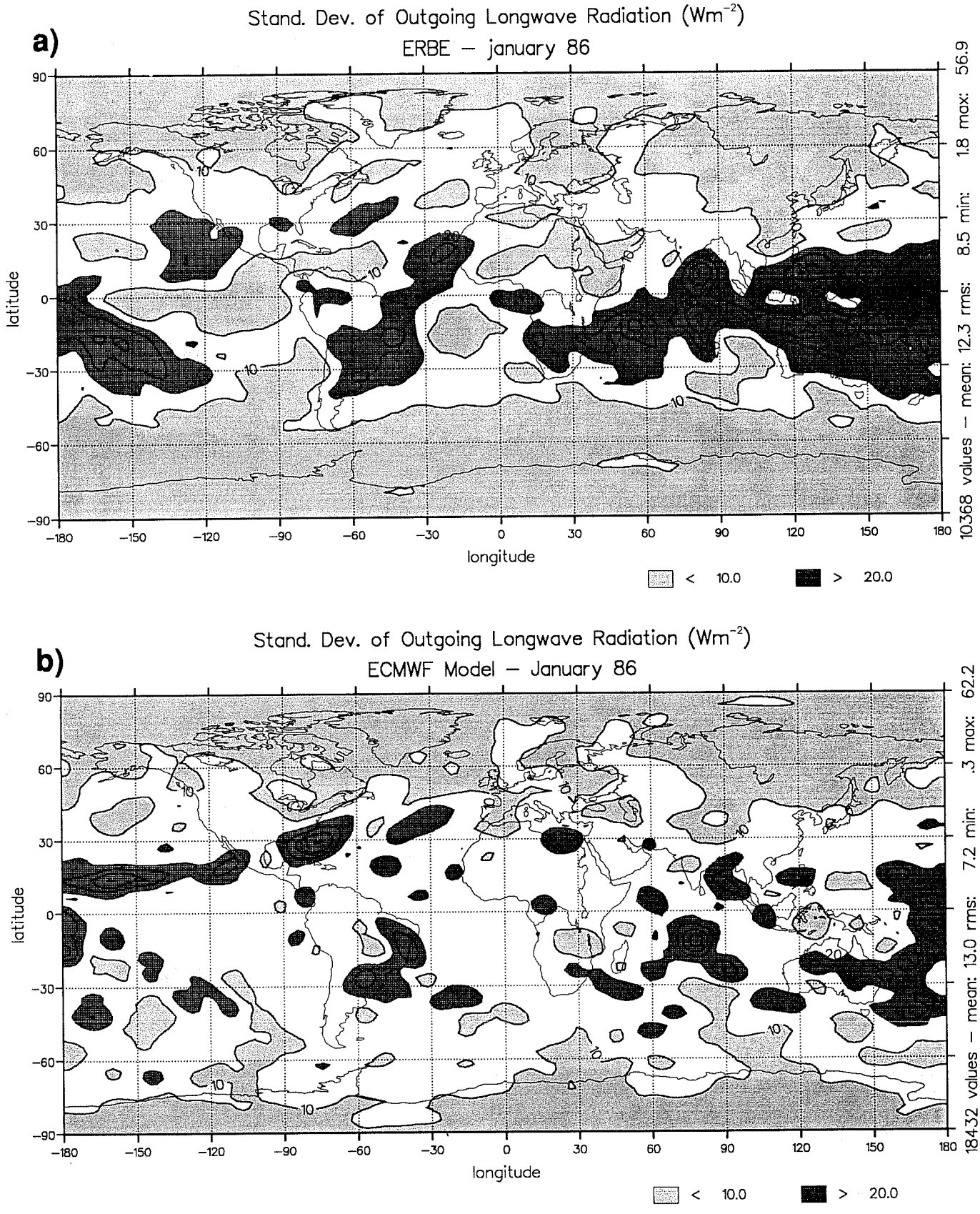

Figure 6: The temporal standard deviation of the outgoing longwave radiation for January 1986: ERBE observations on top (fig.6a), ECMWF model field below (Fig. 6b). Interval is 10 W m^{-2}. Values below 10 W m^{-2} and above 20 W m^{-2} are shaded.

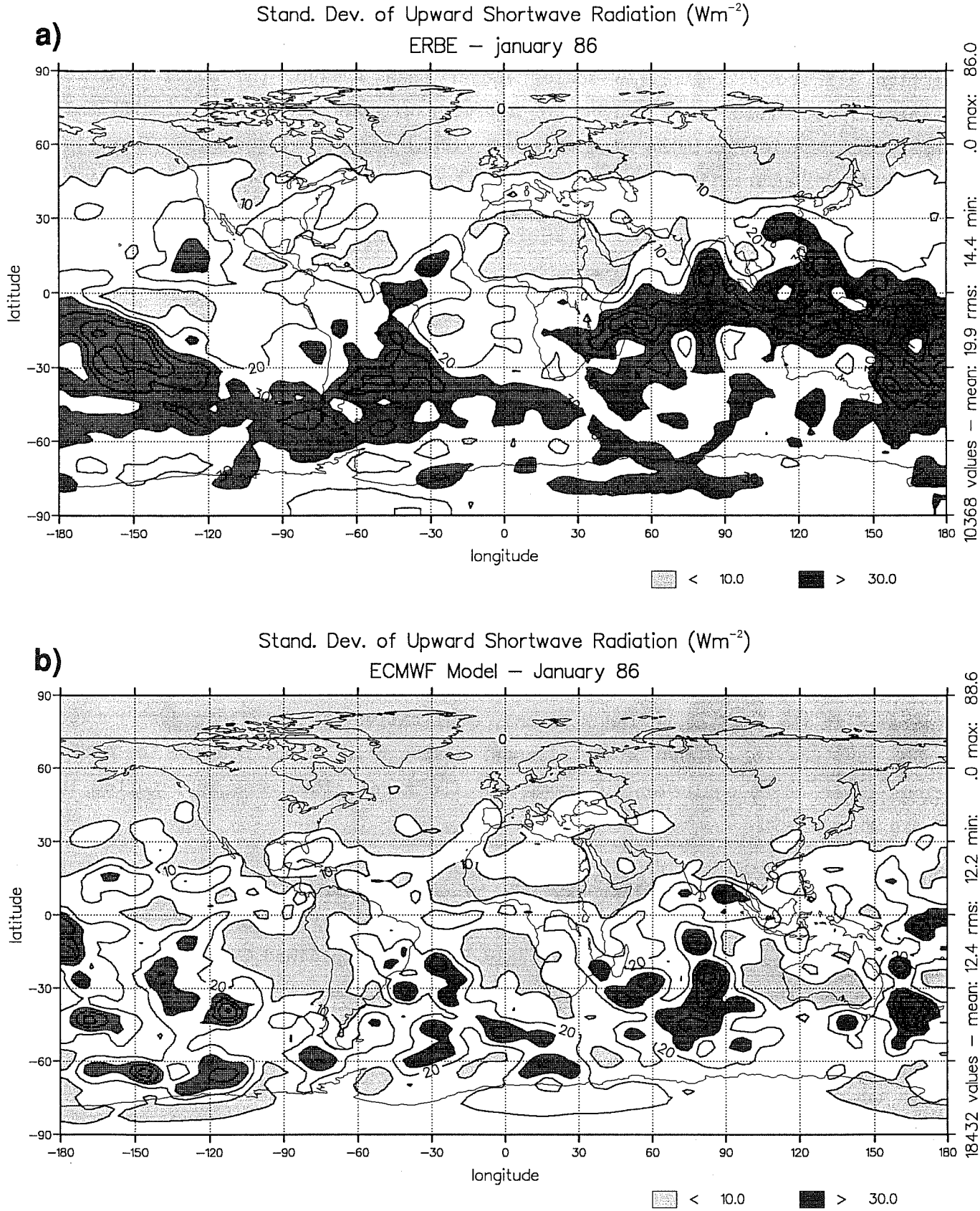

Figure 7: The temporal standard deviation of the upward shortwave radiation for January 1986: ERBE observations on top (fig.7a), ECMWF model field below (Fig. 7b). Interval is 10 W m^{-2}. Values below 10 W m^{-2} and above 30 W m^{-2} are shaded.

This is particularly puzzling as clouds have a too large radiative impact in that area as indicated by the longwave and shortwave cloud forcing maps in section 2.1 and 2.2. On time scales longer than 3 days, the model seem to maintain too persistent a convective activity without any of the significant shifts in location that the high observed σ(OLR) and σ(USW) indicate. There is also a large underestimation of σ(USW) by the model in the 50°S-70°S latitude band. The lack of stratiform clouds west of the tropical continents of the Southern hemisphere also appear in the model low values of σ(USW) (< 10 W m^{-2} instead of the observed 25 W m^{-2}).

3. Regional aspects

Table 1 presents the monthly mean radiative components spatially averaged over some characteristic regions and the coresponding *spatial* standard deviation of the monthly mean radiative components over the same areas. It must first be noted that the model horizontal resolution, $(1.875°)^2$, is slightly higher than that of the ERBE observations, $(2.5°)^2$; therefore we can expect the model standard deviations to be somewhat larger. Six areas have been chosen: the North Atlantic storm track region where the model and observations are in good agreement for all considered parameters, and five areas where deficiencies show up in the map comparisons of section 2. The cloudiness information included in the ERBE scene index is only qualitative. The pixel is just ranked among four possible cloudy state classes. Although we cannot compare the model cloud cover to an equivalent observation, the model cloudiness is reported in Table 1.

In all areas, the model clear-sky USW is underestimated. Differences amount from 2 to 5 W m^{-2} (5 to 10 %) over all oceanic areas, to more than 20 W m^{-2} (40 %) over Brazil. Over the ocean, this might be explained by the absence of aerosols in the model and at higher latitudes (storm track regions of the Northern and Southern hemispheres) by the absence of any dependence of the model ocean surface albedo on the surface wind. Over South America, comparison with another surface albedo climatology (Dorman and Sellers, 1989) has shown the ECMWF albedo to be quite low in that area (0.10 instead of 0.18). As noted in section 2.2, this results in overestimating the SW cloud forcing by the same amount. Over Brazil where the difference is about 30 W m^{-2}, most of it (22 W m^{-2}) could be attributed to a deficient model surface albedo. However, compensating effects may hide more complex deficiencies in cloudy

Table 1: Spatial statistics of observed and model monthly mean radiation fields over characteristic regions. ERBE values are on the left side of each column, model values (between brackets) are on the right side. All quantities are in W m^{-2}.

South Pacific Convergence Zone 180°W - 110°W, 10°S - 30°S	Spatial Mean Value		Spatial Standard Deviation	
clear-sky OLR	284.7	(293.9)	4.3	(8.6)
clear-sky upward SW	49.7	(47.4)	2.0	(1.7)
LW cloud forcing	39.0	(49.6)	21.3	(30.3)
SW cloud forcing	-58.2	(-107.9)	29.1	(40.9)
Net cloud forcing	-19.3	(-58.3)	10.7	(26.7)
Cloudiness		(63.5)		(17.4)

Brazil 70°W - 40°W, 5°S - 20°S	Spatial Mean Value		Spatial Standard Deviation	
clear-sky OLR	284.2	(286.0)	7.7	(8.7)
clear-sky upward SW	74.3	(52.2)	10.0	(6.1)
LW cloud forcing	60.4	(70.7)	14.6	(19.5)
SW cloud forcing	-83.9	(-113.3)	22.4	(44.2)
Net cloud forcing	-17.4	(-42.7)	12.9	(27.9)
Cloudiness		(69.3)		(13.6)

Indonesian Monsoon 90°E - 180°E, 10°N - 20°S	Spatial Mean Value		Spatial Standard Deviation	
clear-sky OLR	286.8	(298.5)	6.9	(9.0)
clear-sky upward SW	49.6	(44.0)	11.8	(5.1)
LW cloud forcing	69.7	(63.4)	25.0	(35.0)
SW cloud forcing	-79.6	(-90.9)	27.9	(52.9)
Net cloud forcing	-9.2	(-27.4)	14.3	(25.8)
Cloudiness		(59.2)		(23.4)

North Atlantic storm track 80°W - 30°W, 50°N - 20°N	Spatial Mean Value		Spatial Standard Deviation	
clear-sky OLR	268.0	(266.6)	23.8	(27.5)
clear-sky upward SW	35.4	(30.5)	9.3	(15.0)
LW cloud forcing	35.6	(39.5)	18.4	(18.4)
SW cloud forcing	-33.2	(-34.1)	16.9	(21.8)
Net cloud forcing	2.5	(5.4)	9.1	(23.0)
Cloudiness		(57.0)		(16.7)

Table 1: (continued)

Western Façade of Peru 100°W - 75°W, 15°S - 40°S	Spatial Mean Value		Spatial Standard Deviation	
clear-sky OLR	282.8	(301.4)	7.5	(12.1)
clear-sky upward SW	52.8	(48.9)	2.3	(1.9)
LW cloud forcing	17.1	(5.1)	5.4	(7.4)
SW cloud forcing	-68.2	(-23.6)	20.5	(24.0)
Net cloud forcing	-44.1	(-18.5)	18.2	(18.0)
Cloudiness		(16.8)		(13.0)

Southern Hemisphere storm tracks 180°W - 180°E, 50°S - 70°S	Spatial Mean Value		Spatial Standard Deviation	
clear-sky OLR	237.3	(240.3)	16.7	(5.1)
clear-sky upward SW	95.6	(86.7)	88.6	(63.8)
LW cloud forcing	28.8	(24.5)	10.2	(4.6)
SW cloud forcing	-128.6	(-50.7)	54.9	(15.3)
Net cloud forcing	-100.4	(-26.1)	46.0	(12.3)
Cloudiness		(60.2)		(8.1)

conditions. Over the SPCZ, in any case, the difference between observed and model SW cloud forcing (about 50 W m^{-2}) cannot be explained by surface albedo problems.

The model clear-sky OLR is overestimated in the SPCZ, Indonesian monsoon and Off-shore Peru areas. In the tropical regions, reasons for this feature have been discussed in section 2.1. A better agreement between model and observed clear-sky OLR is obtained in the storm tracks of both hemispheres and over Brazil. Over the ocean, it might reflect a better humidity field in the PBL at higher latitudes as the model surface winds are stronger and the evaporation is more realistically represented. Over Brazil, the agreement is certainly obtained for the wrong reason, because of a too low model surface temperature. Almost permanent precipitation over this area saturates the model soil moisture and prevents the surface temperature from undergoing a realistic diurnal cycle.

Off-shore Peru where the model cloudiness is 16 %, the lack of stratiform clouds clearly appears in the underestimation by a factor 3 of the model LW and SW cloud forcings.

The too transparent clouds in the Southern storm tracks is seen in the underestimation of the SW cloud forcing. The relatively good agreement between model and observed OLR indicates that the model cloud cover in that area (60.2 % with a spatial homogeneity σ_{cc} of 8 %) is not much smaller than observed. The contrast between LW and SW results is consistent with an explanation based on too small liquid water content for the clouds as the cloud albedo grows more slowly with the cloud liquid water path than the longwave emissivity does. Thus a too small liquid water content will affect more the SW than the LW cloud forcing.

Over areas where convective activity prevails (SPCZ, Brazil, Indonesian monsoon), the radiative impact of the model cloudiness is too large with respect to observations, specially the SW cloud forcing overestimated by the model by as much as 40 % over Brazil. However, it must be stressed that (1) the values derived from the ERBE observations can also be questioned as clear-sky data are missing in areas of the ITCZ where the cloud forcing is likely to be large, and (2) a too small surface albedo adds to the problem.

With respect to spatial variability within the regions considered in Table 1, the model generally displays more spatial structure than the observations. As already mentioned, this is partly due to the different horizontal resolution, but in the convective areas also to the weaker large-scale organization of the model clouds and to their large radiative impact, specially in the shortwave. Over these areas, the discrepancies between observed and model SW and LW cloud forcings do not compensate as shown in the net (LW+SW) cloud forcing. The observed and model net cloud forcings differ over the convective areas by large values (between 18 and 38 W m^{-2}) with a tendency for model clouds to cool the atmosphere too much. Off-shore Peru, the underestimation of the stratiform cloudiness gives a local relative heating of the atmospheric column by 26 W m^{-2} (about 0.2 K day^{-1}). Similarly, the deficiencies in the representation of the Southern hemisphere storm track cloudiness gives a relative heating by 74 W m^{-2} (about 0.65 K day^{-1}).

Conclusion

This comparison of monthly mean modeled and observed radiation fields for January gives some insight about how the cloud-radiation interactions are handled in the ECMWF model. It shows the good representation of the clouds in the storm tracks of the Northern hemisphere; it also points at some overestimation of both the shortwave and longwave impacts of clouds in convective areas, at a lack of low-level stratiform clouds on the western façades of the subtropical continents, and at an underestimation of the radiative impact of the clouds in the higher latitudes of the Southern hemisphere. Except for the common overestimation of clear-sky OLR over the subtropical oceans and lack of low-level stratiform clouds, our results are quite different from those of Kiehl and Ramanathan (1990). This is not surprising given the large differences in the model configurations (in particular with respect to the horizontal resolution and convection and cloud schemes).

The cloud forcing approach provides useful information on the gross characteristics of the clouds. However, more detailed diagnostics are necessary to desentangle the respective role of potential deficiencies in cloud cover, height, ice/liquid water content and optical properties in the differences shed into light by this study.

It is also necessary to complement this study by comparing observations and model outputs on smaller spatial and temporal scales. An agreement on the monthly means does not guarantee a proper representation of either the inter- or intradiurnal variability which is highly relevant for weather forecasts. If improvement in parameterization of cloud-radiation interactions is to be expected from such comparisons, one must distinguish between the different regional weather régimes with respect to their persistence or higher temporal variability. Finally, similar comparisons should be repeated for other seasons as different large-scale forcings (Asian summer monsoon in particular) might reveal other problems in the model.

REFERENCE

Barkström, B.R., 1984: The Earth Radiation Budget Experiment. *Bull. Amer. Meteor. Soc.*, **65**, 1170-1185.

Barkström, B.R., and G.L. Smith, 1986: The Earth Radiation Budget Experiment: Science and implementation. *Rev. Geophys.*, **24**, 379-390.

Beljaars, A., and M. Miller, 1990: The sensitivity of the ECMWF model to the parametrization of evaporation from the tropical oceans. *ECMWF Research Dept. Technical Memo.* **170**, 18 pp.

Cess, R.D., G.L. Potter, J.-P. Blanchet, G.J. Boer, S.J. Ghan, J.T. Kiehl, H. Le Treut, Z.X. Li, Z.-X. Liang, J.F.B. Mitchell, J.-J. Morcrette, D.A. Randall, M.R. Riches, E. Roeckner, U. Schlese, A. Slingo, K.E. Taylor, W.M. Washington, R.T. Wetherald, and I. Yagai, 1989: Interpretation of cloud-climate feedback as produced by 14 atmospheric general circulation models. *Science*, **245**, 513-516.

Coakley, J.A., Jr., and D.G. Baldwin, 1984: Towards the objective analysis of clouds from satellite imagery data. *J. Clim. Appl. Meteor.*, **23**, 1065-1099.

Dorman, J.L., and P.J. Sellers, 1989: A global climatology of albedo, roughness length and stomatal resistance for atmospheric general circulation models as represented by the Simple Biosphere model (SiB). *J. Appl. Meteor.*, **28**, 833-855.

Fouquart, Y., and B. Bonnel, 1980: Computations of solar heating of the Earth's atmosphere: A new parameterization. *Beitr. Phys. Atmosph.*, **53**, 35-62.

Geleyn, J.-F., and H.-J. Preuss, 1983: A new data set of satellite-derived surface albedo values for operational use at ECMWF. *Arch. Meteor. Geophys. Bioclim.*, **32A**, 353-359.

Kiehl, J.T., and V. Ramanathan, 1990: Comparison of cloud forcing derived from the Earth Radiation Budget Experiment with that simulated by the NCAR Community Climate Model. *J. Geophys. Res.*, **95D**, 11,679-11,698.

Mitchell, J., 1989: The "greenhouse" effect and climate change. *Rev. Geophys.*, **27**, 115-140.

Morcrette, J.-J., 1990a: Impact of changes to the radiation transfer parameterizations plus cloud optical properties in the ECMWF model. *mon. Wea. Rev.*, **118**, 847-873.

Morcrette, J.-J., 1990b: Radiation and cloud radiative properties in the ECMWF forecasting system. *J. Geophys. Res.*, **95D**, in press.

Morcrette, J.-J., and Y. Fouquart, 1985: On systematic errors in parametrized calculations of longwave radiation transfer. *Quart. J. Roy. Meteor. Soc.*, **111**, 691-708.

Morcrette, J.-J., and Y. Fouquart, 1986: The overlapping of cloud layers in shortwave radiation parameterizations. *J. Atmos. Sci.*, **43**, 321-328.

Morcrette, J.-J., and Y. Fouquart, 1989: Comparison of E.R.B.E. measurements with model-generated radiation fields. *IRS'88: Current Problems in Atmospheric Radiation*, J. Lenoble and J.-F. Geleyn, Eds., A. Deepak Publish., Hampton, Va., 332-334.

Morcrette, J.-J., L.D. Smith, and Y. Fouquart, 1986: Pressure and temperature dependence of the absorption in longwave radiation parameterizations. *Beitr. Phys. Atmosph.*, **59**, 455-469.

Slingo, J.M., 1987: The development and verification of a cloud prediction scheme for the ECMWF model. *Quart. J. Roy. Meteor. Soc.*, **113**, 899-928.

Smith, G.L., R.N. Green, E. Raschke, L.M. Avis, J.T. Suttles, B.A. Wielicki, and R. Davies, 1986: Inversion methods for satellite studies of the earth radiation budget: Development of algorithms for the ERBE mission. *Rev. Geophys.*, **24**, 407-421.

Smith, L.D., 1989: Satellite versus GCM-simulated radiation balance: Comparisons and implications for climate modelling. *Ph.D. Thesis*, Dept. of Atmospheric Sciences, Colorado State Univ., Fort Collins, Colorado, 308 pp.

Tiedtke, M., 1989: A comprehensive mass-flux scheme for cumulus parameterization in large-scale models. *Mon. Wea. Rev.*, **117**, 1779-1800.